Cavity enhanced third harmonic generation in graphene

Chris Beckerleg, Thomas J. Constant, Ioannis Zeimpekis, Samuel M. Hornett, Chris Craig, Daniel W. Hewak, and Euan Hendry

---

Cavity enhanced third harmonic generation in graphene

Chris Beckerleg,[1,a)] Thomas J. Constant,[1] Ioannis Zeimpekis,[2] Samuel M. Hornett,[1] Chris Craig,[2] Daniel W. Hewak,[2] and Euan Hendry[1]

[1]*Physics Department, University of Exeter, Exeter EX4 4QL, United Kingdom*
[2]*Physics Department, University of Southampton, Southampton SO17 1BJ, United Kingdom*

Graphene displays a surprisingly large third order nonlinearity. Here, we report that conversion efficiencies approaching 10^{-4} are possible for third harmonic generation (THG). Moreover, the atomically thin nature of graphene allows for simple integration in cavity designs to increase this even further. We demonstrate a 117-fold enhancement, of resonant vs non-resonant wavelengths in the THG from graphene due to the integration of a graphene layer with a resonant cavity. This large enhancement occurs as the cavity is resonant for both the fundamental field and the third harmonic. We model this effect using the finite difference time domain approach. By comparing our model with experiment, we are able to deduce the value of a bulk third order susceptibility of graphene of $|\chi^{(3)}| = 4 \times 10^{-17} (\text{m/V})^2$. © 2018 Author(s). All article content, except where otherwise noted, is licensed under a Creative Commons Attribution (CC BY) license (http://creativecommons.org/licenses/by/4.0/). https://doi.org/10.1063/1.4999054

Graphene is a very promising material for future applications in optoelectronics and photonics.[1] In the visible spectral range, many of the interesting photonic properties of graphene arise due to its linear band structure,[2] which infers a wide operation bandwidth in terms of its linear and nonlinear optical properties.[3] Meanwhile, at infra-red frequencies, surface plasmons have been experimentally demonstrated[4,5] and their frequency response was controlled through the application of an external bias.[6] As a result, graphene is being considered for numerous applications, such as solar-cells and displays,[7] which aim to exploit the combination of a highly conductive yet transparent single layer. Additionally, the broad absorption spectrum of graphene also highlights its potential for photodetection applications.[8]

A single layer of graphene is relatively transparent, absorbing only 2.3% of incident visible light.[9] However, this low absorption occurs due to the atomically thin nature of graphene, not due to a weak electromagnetic interaction. Moreover, the nonlinear optical interactions with graphene are known to be surprisingly large.[10–12] To date, there have been several experiments and theoretical investigations into the various nonlinear processes in graphene, from two photon absorption[13] to difference frequency generation.[14] This work focuses on third harmonic generation, which is described with a third order susceptibility $\chi^{(3)}$. Mikhailov predicted that the third order susceptibility of graphene is large, especially in comparison to dielectric materials.[15,16] Meanwhile, third harmonic generation in graphene has been experimentally investigated in mechanically exfoliated graphene flakes by Kumar *et al.*[10] and Hong *et al.*[17] Theoretically, third harmonic generation has been studied by Cheng *et al.* with a perturbative calculation.[18] Fourwave mixing, also a third order process, has been measured[11] and studied theoretically by Zhang *et al.*, with a quantum-dynamical theory.[19]

Whilst these studies report a comparatively large value of $\chi^{(3)}$ in graphene, the absolute energy conversion is limited by the atomically thin nature of graphene. Therefore, methods for enhancing the nonlinear effects are desirable. One such approach to enhance these nonlinear interactions in graphene is to utilise a planar cavity. To exploit this, Savostianova and Mikhailov theoretically proposed the use of a layered structure, consisting of a graphene layer combined with a dielectric on top of a gold film.[20] Compared to utilising surface plasmons, a previously demonstrated method of enhancing nonlinearity,[21] a layered structure removes the precise requirements on the frequency and wavevector for coupling incident photons to surface plasmons. Such a planar cavity is predicted to enhance the third harmonic generation from graphene by up to two orders of magnitude.[20]

In this work, we measure the third harmonic generation from a graphene topped planar cavity, one specifically designed for this purpose. We use finite difference time domain (FDTD) numerical modelling to describe both the linear and nonlinear properties of the system simultaneously, allowing cavity dimensions and thickness to be optimised,[22,23] as shown in Fig. 1(a). We then characterize the integrated cavity in experiment, recording the intensity of generated third harmonic as a function of incident wavelength. By comparing the graphene integrated cavity and the cavity by itself, we also demonstrate that the third harmonic signal originates almost entirely from the graphene layer. A clear 117-fold enhancement in the normalised third harmonic power is observed at the resonant wavelength, relative to the third harmonic power for non-resonant wavelengths. Finally, by comparing our measurements to our FDTD simulations, we are able to deduce a value of the bulk third order susceptibility of our graphene of $|\chi^{(3)}| = 4 \times 10^{-17} (\text{m/V})^2$.

First, we begin by introducing our FDTD model. As is convention, we define the linear optical response of our graphene layer through a surface conductivity, σ_g. However, for modelling purposes and to allow comparison to the literature, we can convert to equivalent bulk properties using

a)Also at Physics Department, University of Exeter, Exeter EX4 4QL, United Kingdom. Electronic mail: cb362@ex.ac.uk
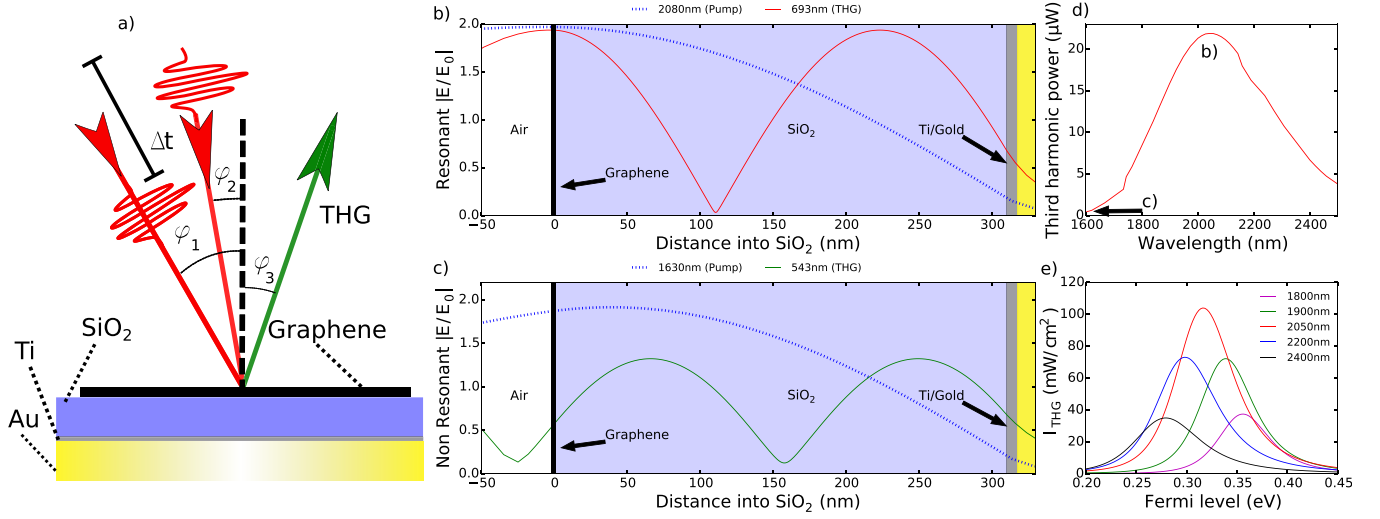
FIG. 1. (a) Schematic diagram of the experimental geometry and sample structure showing the two incident pulses separated by a variable delay time, Δt. The incident angles of incidence are $\phi_2 = 8°$, while the third harmonic signal is measured at $\phi_1 = 30°$. The measured third harmonic signal is generated at $\phi_3 = 15°$. The thickness of the layers is Au: 150 nm, Ti: 8 nm, and SiO$_2$: 309 nm. (b) FDTD modelling of the electric field profile through the stack at the resonance condition. The incident wavelength is 2080 nm (blue dotted line) and the third harmonic wavelength is 693 nm (red solid line). (c) FDTD modelling of the electric field profile through the sample away from the resonance condition. The incident wavelength is 1630 nm (solid green line) and a third harmonic wavelength is 543 nm (dotted blue). (d) FDTD modelling prediction of third harmonic generated as a function of the incident wavelength. The wavelengths of the FDTD electric field profiles in (b) and (c) are labelled. (e) Theoretical prediction of how the third harmonic intensity of the cavity changes a function of the Fermi level of the graphene for a selection of incident wavelengths, 2400 nm black, 2200 nm blue, 2050 nm red, 1900 nm green, and 1800 nm magenta, assuming a relaxation time of $\approx$10 fs.[35]

$$1 + \chi^{(1)} = \epsilon_b + \frac{i\sigma_g}{\epsilon_0 \omega \Lambda}, \quad (1)$$

where $\chi^{(1)}$ is the bulk susceptibility, ω is the frequency, ϵ_0 is the permittivity of free space, $\epsilon_b = 2.5$ is the background permittivity,[24] and $\Lambda = 0.3$ nm is the thickness of the graphene sheet (as determined by ellipsometry measurements[25]). By applying the Kubo formula to graphene and assuming $k_b T \ll E_f$, the sheet conductivity of the graphene, σ_g, can be expressed as[26–28]

$$\sigma_g = \frac{ie^2 E_f}{\pi \hbar (\omega + i\tau^{-1})}$$
$$+ \frac{e^2}{4\hbar} \left[\Theta(\hbar\omega - 2E_f) + \frac{i}{\pi} \log_{10} \left| \frac{\hbar\omega - 2E_f}{\hbar\omega + 2E_f} \right| \right]. \quad (2)$$

This expression accounts for both interband and intraband transitions in the graphene layer. The scattering rate, τ, is defined as, $\tau = E_f \mu / e v_f^2$, $\omega = 2\pi f$ where f is the frequency. Θ is the Heaviside step function. The Fermi energy, $E_f = 0.2$ eV, and mobility, $\mu = 1000$ cm^2 V^{-1} s^{-1}, are set to values typical for chemical vapor deposition (CVD) graphene.[5,29] Our cavity is formed from a dielectric layer of SiO$_2$, thickness = 310 nm, and a conducting layer of gold, thickness = 150 nm, as depicted in Fig. 1(a); the optical responses of these materials are wavelength dependent, as described by Palik.[30] In our experimental sample, a thin (8 nm) layer of titanium is required for adhesion, and this layer is also included in our model for completeness. The entire structure is modelled in 2D, assuming periodic boundary conditions in the planar directions. A vacuum box of 8 μm depth perpendicular to the graphene by 200 nm in the plane of the graphene is included on the incident half space. Note that, since the gold layer is optically thick, we do not

require a vacuum box in the transmission half space. A rectangular, conformal mesh is imposed on the entire structure, with a minimum mesh size of 0.025 nm. The wavelength dependent reflection of the cavity is calculated using a broad band pulse and by integrating the Poynting vector, through a plane parallel to the graphene layer, 2 μm away from the surface. The nature of the FDTD method allows the fields inside the cavity for different wavelengths to be determined and is shown in Figs. 1(b) and 1(c).

Nonlinearity is introduced into the model by expanding the polarisation as a power series, introducing an effective third order susceptibility, $\chi^{(3)}$, as[31]

$$\bar{P} = \epsilon_0 (\chi^{(1)} \bar{E} + \chi^{(3)} \bar{E}^3). \quad (3)$$

Due to the centrosymmetry of graphene, we set $\chi^{(2)} = 0$. Here, we treat $\chi^{(3)}$ as a perturbative fit parameter, allowing us to match the generated third harmonic in our model to that observed in experiment. To simulate as close as possible the experimental conditions, a pulse of a fixed carrier frequency, modulated with a gaussian envelope, was applied to the graphene layer, at normal incidence. This pulse has a full width at half maximum (FWHM) of 100 fs and a peak electric field amplitude of 2.3×10^8 V/m corresponding to an average power of 4.5 mW at the 1.05 kH repetition rate used the experiment. The central wavelength is varied in the range of 1630 nm to 2400 nm. At each input wavelength, the average power of third harmonic power generated is determined by again integrating the Poynting vector across a plane parallel to the graphene, placed 2 μm from the surface. Figure 1(d) shows how the generated third harmonic power is predicted to vary with the input wavelength, which is greatly enhanced at the resonance of the cavity. If we define the cavity enhancement as the ratio of the third harmonic power generated by a pulse with the resonant wavelength of 2080 nm, to

the third harmonic power generated by a pulse with a non-resonant incident wavelength of 1630 nm, we can estimate an enhancement factor of 85. This is comparable to the prediction made by Savostianova and Mikhailov.[20]

Interestingly, a planar graphene-cavity structure provides a possible route for applications where modulation or switching of harmonic generation is required. In recent years, a strong variation in the nonlinearity of graphene with the Fermi level, particularly in the near to mid-infrared range has been predicted.[32–35] While it is not clear precisely how the graphene susceptibility will evolve with the Fermi level, it will certainly be dependent on material parameters such as the relaxation time.[35] Using a relaxation time of 10 fs, typical for CVD graphene,[36–38] we can illustrate representative behaviour of a cavity geometry. In Fig. 1(e), we plot the predicted third harmonic intensity, anticipated for the cavity of Fig. 1(a), as a function of Fermi level for various incident wavelengths, using the predictions of Mikhailov.[35] Figure 1(e) demonstrates that a Fermi level shift of a few hundred meV might be expected to completely modulate the harmonic signal generated from the cavity. Note that this effect arises due to the variable nonlinearity of the graphene itself combined with the frequency dependence of the cavity. We have also modelled the change in the linear cavity response with the Fermi level and found it to be negligible. While our sample design did not allow for such tests, such tunability could, in principal, be brought about through molecular doping or electrical gate control, with potential for impressive switching speeds.[8]

In Figs. 1(b) and 1(c), we plot the time-averaged electric fields calculated for two different cases: on and off resonance. The electric field profile of the resonant incident wavelength, 2080 nm, (blue dotted line) has a maximum at the surface of the graphene layer. The electric field profile of the third harmonic generated by this resonant wavelength, 693 nm (red solid line), also has a maximum at the graphene surface, making the cavity double resonant. This contrasts with a non-resonant case as shown in Fig. 1(c), plotted for an input wavelength of 1630 nm. While the field for the incident wavelength has a smaller magnitude at the surface of the graphene compared to that for the resonant wavelength, the electric field profile of third harmonic wavelength generated (i.e., 543 nm) is reduced by around a factor of four from the resonant condition.

Taking these modelled parameters as a guide, we fabricated a simple cavity on top of a glass microscope slide, used as a support substrate. A 5 nm layer of chrome is thermally evaporated onto the glass to provide an adhesive layer for thermal evaporation of a 150 nm layer of gold. The samples are then cleaned with acetone, IPA, and water and dried. Before the silicon dioxide deposition, the sample is exposed to an argon etch of 1 min at a pressure of 30 mTorr and at 30 W RF power to remove possible contaminants. A second 5 nm Ti adhesion layer is then sputter-coated at a pressure of 2 mTorr and at 300 Ws DC power. Finally, a SiO_2 layer is sputter-coated from a SiO_2 target, with a 2:1 Ar to O_2 gas ratio, at 2 mTorr and at 150 W RF power, using an AJA Orion sputterer. Using ellipsometric measurements, the thicknesses of the Ti and SiO_2 layers were confirmed to be 8 and 309 nm, respectively. A 1 cm × 1 cm area CVD graphene, sourced from graphene-supermarket.com, is then transferred onto the sample using a PMMA assisted transfer technique.[39,40]

To measure the third harmonic generation from this layered structure, we perform a two-pulse correlation measurement which allows a background free characterization of the sample, shown in Fig. 1(a). In this approach, two 1.05 kHz, 100 fs, TM polarised, laser pulses with comparable fluences and a tunable central wavelength, in the range of 1630 nm–2400 nm, are generated using an optical parametric amplifier. These pulses are incident on the sample with angles $\phi_2 = 8°$, $\phi_1 = 30°$, see Fig. 1(a), and are spatially overlapped at the sample interface, spot diameter $\approx 800\,\mu m$. These incident beams were spectrally filtered using a silicon wafer (transmitting for wavelengths > 1130 nm) to remove any optical contamination in the beams. The fluence of the pulses is kept below 1 mJ/cm², well below the photo-modification threshold for graphene.[41] A thermal power meter, measuring the reflection of the incident pulse, allows for continuous monitoring of the average incident power, typically ≈ 6 mW. The temporal overlap of these two beams, Δt, at the sample interface is controlled by a motorized delay stage, changing the path length of one pulse and therefore the arrival time. Using our two-pulse correlation approach, a signal is measured only when the pulses are temporally and spatially overlapped, giving a completely background free signal. The third harmonic signal is expected to be generated at four different angles: $8°, 15°, 23°$, and $30°$ which allows for spatial filtering of the generated third harmonic signal. To measure the harmonic signal, an avalanche photodiode, protected by an 800 nm short pass filter, is placed at $\phi_3 = 15°$ and connected to a lock-in amplifier. One of the incident beams is then modulated at 525 Hz via a mechanical chopper, and the voltage from the lock-in amplifier is recorded. Through characterisation of the detector with a known average power, this voltage can be converted into average power. The sample is mounted on an xyz micrometer stage so that areas of the sample covered with graphene can be easily compared to areas free from graphene.

Figure 2(a) shows a typical measurement of third harmonic power measured as a function of the time delay between pulses for the combined graphene-cavity structure (blue circles). By estimating the transversal time for the crossing wave fronts of the two beams in our non-collinear geometry, we can estimate a minimum expected broadening of the signal. Considering the smallest experimental spot size at the sample $\approx 470\,\mu m$ and $\approx 22°$ between the incident beams, the minimum broadening expected will be $(\approx \sin(22°) 470\mu m)/(c) \approx 600$ fs, where c is the speed of light, consistent with the measurement width in Fig. 2(a). We note that the total third harmonic power generated is expected to be approximately four times the measured power, since there are four possible phase matching angles. We point out that the angular dependence of the cavity resonances will undoubtedly increase the intensity of some phase-matched harmonic beams at the expense of others. For example, for short incident and harmonic wavelengths, we expect the cavity to be closer to resonance for the smallest phase matched angle, and so, one can anticipate that the harmonic beam generated in this direction will be larger than expected, at the expense of the beam generated at the largest phase matching angle. However, since we
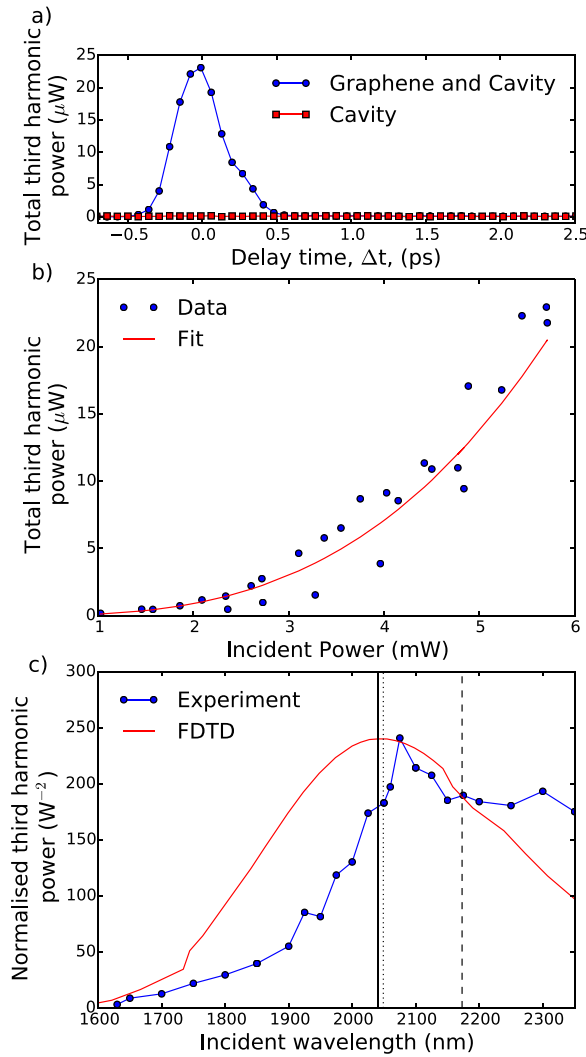
a)

FIG. 2. (a) A typical time delay measurement of the total third harmonic generated, for $\lambda = 2080$ nm, comparing an area on the sample with graphene (blue circles) to the response of just the cavity (red squares), and incident power is 6.5 mW. (b) Third harmonic generation as a function of the average incident power. The red line is a least-squares fit to the measured data points, which is found to be $P_{thg} \propto P_{inc}^{2.98}$. (c) The measured third harmonic power generated by the cavity, normalised to the time-average reflected power, as a function of the incident wavelength, comparing the FDTD modelling results from Fig. 1(d) (red line) with the measured values (blue circles), with a modelled incident power of ≈ 4.5 mW. The shift in the position of the resonance, relative to normal incidence (solid line), is marked for incident angles of 8° (dotted line) and 30° (dashed line).

record one of the central phase matched directions (15° out of 8°, 15°, 23°, and 30°), this effect will be minimized. Therefore, while the factor of four used to normalise our data will only be strictly correct for an angle between the beams that tends to zero, we believe it to be a reasonable approximation of the true scaling factor. For this reason, in Fig. 2, we plot total harmonic power as four times the measured value. The measurement from the cavity alone, red squares in Fig. 2(a), confirms that the third harmonic signal originates predominantly from the graphene. To further investigate the origin of the signal, the total incident power is varied using a neutral density filter; the resulting third harmonic power, P_{thg}, is recorded and shown in Fig. 2(b). P_{thg} is expected to depend on the cube of the incident electric power, P_{inc}. Using a least-squares approach, we find that the best fit to our data is

$P_{thg} \propto P_{inc}^{2.98}$ [red line in Fig. 2(b)]. Furthermore, the signal is also found to be highly sensitive to the angle of detection, disappearing completely within $\approx 1°$ of ϕ_3, as expected for a coherent signal such as third harmonic generation. A huge advantage of our two-pulse measurement approach is therefore the spatial separation of harmonic signal generated from the very thin sample.

The effect of the cavity can be investigated by simultaneously varying the wavelengths of both incident pulses from 1630 nm to 2400 nm and recording the third harmonic power on our detector and the reflected power. Note that the width of the measurement is determined predominantly by cavity resonance, indicating that the relaxation time is smaller than 10 fs. We note that the precise power of the incident beam has a large influence on the magnitude of the measured third harmonic power. For this reason, in Fig. 2(c), we compensate for the wavelength dependent transmission of our 800 nm short pass filter and normalise to the cube of a simultaneous measurement of the reflected power. The non-collinear geometry, required for simultaneous power measurements, increases the effective path length inside the cavity compared to normal incidence. The increase in the effective path length leads to the observed shift in the resonance to longer wavelengths as shown in the difference between the modelling prediction (red line) and measurement (blue lines) in Fig. 2(c). Using Snell's law, the position of the resonance at 8° (dotted line) and 30° (dashed line) is marked in Fig. 2(c), shown relative to normal incidence (solid line). By comparing the measured harmonic signal on (2080 nm) and off (1630 nm) resonance, we estimate an enhancement factor of 117. This is in reasonable agreement with the value of 85 extracted from FDTD simulations and with the estimates made by Savostianova and Mikhailov.[20]

To best match the absolute power measured in experiment, we require a bulk susceptibility in our model of $|\chi^{(3)}| = 4 \times 10^{-17} (\text{m/V})^2$. While the value of $\chi^{(3)}$ depends on the specific nonlinear process, with large values for $\chi^{(3)}$ being reported in fourwave mixing experiments,[11] the value of $\chi^{(3)}$ reported here is comparable to the values obtained for the third harmonic generation experiments performed by Kumar *et al.* $[|\chi^{(3)}| = 4 \times 10^{-17}, 8 \times 10^{-17} (\text{m/V})^2]$[10] and the theoretical prediction of fourwave mixing by Zhang *et al.* $[\chi^{(3)} = 2 \times 10^{-17} (\text{m/V})^2]$,[19] though the susceptibility is expected to be Fermi level dependent. However, it is considerably larger than the prediction for third harmonic generation by Cheng *et al.* $[|\chi^{(3)}| = 6 \times 10^{-19} (\text{m/V})^2]$.[18] As noted by Cheng *et al.* themselves, this discrepancy may arise from a breakdown of the linear dispersion approximations, non-equilibrium electron dynamics, or thermal effects, all of which are not treated in their perturbative model. Note that, with the surprisingly strong cavity effect reported here, we observe a harmonic photon conversion efficiency of 4×10^{-3} for the largest powers used. For essentially a planar structure, such high conversion efficiencies could be useful in applications where velocity phase matching in bulk crystals is unachievable.

In conclusion, we have shown that graphene displays surprisingly large third order nonlinearity when placed in a planar cavity. We demonstrate a 117-fold enhancement in the third harmonic generation from graphene due to the integration of a graphene layer with a resonant cavity. This rather

large enhancement occurs as the cavity is resonant for both the fundamental field and the third harmonic field. By modelling this effect using the finite difference time domain approach, we deduce a bulk third order susceptibility of graphene of $|\chi^{(3)}| = 4 \times 10^{-17} (\text{m/V})^2$.

[1]K. S. Novoselov, A. K. Geim, S. V. Morozov, D. Jiang, Y. Zhang, S. V. Dubonos, I. V. Grigorieva, and A. A. Firsov, Science **306**, 666 (2004).

[2]A. K. Geim and K. S. Novoselov, Nat. Mater. **6**, 183 (2007).

[3]J. M. Dawlaty, S. Shivaraman, J. Strait, P. George, M. Chandrashekhar, F. Rana, M. G. Spencer, D. Veksler, and Y. Chen, Appl. Phys. Lett. **93**, 3 (2008).

[4]E. H. Hwang and S. Das Sarma, Phys. Rev. B **75**, 205418 (2007).

[5]L. Ju, B. Geng, J. Horng, C. Girit, M. Martin, Z. Hao, H. A. Bechtel, X. Liang, A. Zettl, Y. R. Shen, and F. Wang, Nat. Nanotechnol. **6**, 630 (2011).

[6]Z. Fei, A. S. Rodin, G. O. Andreev, W. Bao, A. S. McLeod, M. Wagner, L. M. Zhang, Z. Zhao, M. Thiemens, G. Dominguez, M. M. Fogler, A. H. Castro Neto, C. N. Lau, F. Keilmann, and D. N. Basov, Nature **487**, 82 (2012).

[7]F. Bonaccorso, Z. Sun, T. Hasan, and A. C. Ferrari, Nat. Photonics **4**, 611 (2010).

[8]F. Xia, T. Mueller, Y. M. Lin, A. Valdes-Garcia, and P. Avouris, Nat. Nanotechnol. **4**, 839 (2009).

[9]R. R. Nair, P. Blake, A. N. Grigorenko, K. S. Novoselov, T. J. Booth, T. Stauber, N. M. R. Peres, and A. K. Geim, Science **320**, 1308 (2008).

[10]N. Kumar, J. Kumar, C. Gerstenkorn, R. Wang, H. Y. Chiu, A. L. Smirl, and H. Zhao, Phys. Rev. B **87**, 121406 (2013).

[11]E. Hendry, P. J. Hale, J. Moger, A. K. Savchenko, and S. A. Mikhailov, Phys. Rev. Lett. **105**, 097401 (2010).

[12]S. A. Mikhailov, Phys. E **44**, 924 (2012).

[13]Z. Liu, Y. Wang, X. Zhang, Y. Xu, Y. Chen, and J. Tian, Appl. Phys. Lett. **94**, 021902 (2009).

[14]T. Gu, N. Petrone, J. F. McMillan, A. V. Zande, M. Yu, G. Q. Lo, D. L. L. Kwong, J. Hone, and C. W. Wong, Nat. Photonics **6**, 554 (2012).

[15]R. Hellwarth, Prog. Quantum Electron. **5**, 1 (1977).

[16]S. A. Mikhailov, Europhys. Lett. **79**, 27002 (2007).

[17]S. Y. Hong, J. I. Dadap, N. Petrone, P. C. Yeh, J. Hone, and R. M. Osgood, Phys. Rev. X **3**, 021014 (2013).

[18]J. L. Cheng, N. Vermeulen, and J. E. Sipe, New J. Phys. **18**, 029501 (2014).

[19]Z. Zhang and P. L. Voss, Opt. Lett. **36**, 4569 (2011).

[20]N. A. Savostianova and S. A. Mikhailov, Appl. Phys. Lett. **107**, 181104 (2015).

[21]T. J. Constant, S. M. Hornett, D. E. Chang, and E. Hendry, Nat. Phys. **12**, 124 (2015).

[22]C. Beckerleg and E. Hendry, J. Opt. Soc. Am. B **33**, 2051 (2016).

[23]See http://www.lumerical.com/tcad-products/fdtd/ for Lumerical Solutions Inc.

[24]E. Şaşioğlu, H. Hadipour, C. Friedrich, S. Blügel, and I. Mertig, Phys. Rev. B **95**, 060408 (2017).

[25]J. W. Weber, V. E. Calado, and M. C. M. van de Sanden, Appl. Phys. Lett. **97**, 091904 (2010).

[26]B. Wunsch, T. Stauber, F. Sols, and F. Guinea, New J. Phys. **8**, 318 (2006).

[27]L. A. Falkovsky, J. Phys.: Conf. Ser. **129**, 012004 (2008).

[28]T. Stauber, N. M. R. Peres, and A. K. Geim, Phys. Rev. B **78**, 085432 (2008).

[29]A. Pirkle, J. Chan, A. Venugopal, D. Hinojos, C. W. Magnuson, S. McDonnell, L. Colombo, E. M. Vogel, R. S. Ruoff, and R. M. Wallace, Appl. Phys. Lett. **99**, 122108 (2011).

[30]E. D. Palik, *Handbook of Optical Constants of Solids* (Academic press, 1998).

[31]R. Boyd, *Handbook of Laser Technology and Applications*, 3rd ed. (Taylor & Francis, 1992).

[32]J. L. Cheng, N. Vermeulen, and J. E. Sipe, Phys. Rev. B **91**, 235320 (2015).

[33]V. Margulis, E. Muryumin, and E. Gaiduk, Phys. Lett. A **380**, 304 (2016).

[34]B. Semnani, A. H. Majedi, and S. Safavi-Naeini, J. Optics **18**, 035402 (2016).

[35]S. A. Mikhailov, Phys. Rev. B **90**, 241301 (2014).

[36]B. D. Kong, J. G. Champlain, and J. B. Boos, J. Appl. Phys. **121**, 235101 (2017).

[37]K. F. Mak, L. Ju, F. Wang, and T. F. Heinz, Solid State Commun. **152**, 1341 (2012).

[38]A. Reina, X. Jia, J. Ho, D. Nezich, H. Son, V. Bulovic, M. S. Dresselhaus, and J. Kong, Nano Lett. **9**, 30 (2009).

[39]X. Li, Y. Zhu, W. Cai, M. Borysiak, B. Han, D. Chen, R. D. Piner, L. Colombo, and R. S. Ruoff, Nano Lett. **9**, 4359 (2009).

[40]X. Liang, B. A. Sperling, I. Calizo, G. Cheng, C. A. Hacker, Q. Zhang, Y. Obeng, K. Yan, H. Peng, Q. Li, X. Zhu, H. Yuan, A. R. H. Walker, Z. Liu, L. M. Peng, and C. A. Richter, ACS Nano **5**, 9144 (2011).

[41]E. Alexeev, J. Moger, and E. Hendry, Appl. Phys. Lett. **103**, 151907 (2013).